ELSEVIER

Journal of Alloys and Compounds 443 (2007) 149–154

Journal of ALLOYS AND COMPOUNDS

www.elsevier.com/locate/jallcom

Particle size effect on formation and stability of β-$La_2Mo_2O_9$ ionic conductor

R.A. Rocha, E.N.S. Muccillo *

Instituto de Pesquisas Energéticas e Nucleares, CCTM, Centro Multidisciplinar para o Desenvolvimento de Materiais Cerâmicos, R. do Matão, Trav. R 400, Cidade Universitária, Sao Paulo 05508-000, SP, Brazil

Received 3 February 2006; received in revised form 30 September 2006; accepted 2 October 2006
Available online 31 October 2006

Abstract

The $La_2Mo_2O_9$ compound was prepared by thermal crystallization from a mixed nitrate solution to obtain a precursor material with different particle size than that obtained by the conventional mixing of starting oxides. This precursor material was characterized by several techniques before and after thermal decomposition into the final compound. X-ray diffraction and electron microscopy results evidence the formation of the high-temperature β-$La_2Mo_2O_9$ phase after calcination at 550 °C. The well-known α-to-β phase transition was detected at temperatures lower than that for powders prepared from mixing of starting oxides. Electrical conductivity measurements at several oxygen partial pressures show that specimens prepared from nitrates have a different behavior when compared to those specimens obtained by the conventional route. The overall results reveal the role of particle size of the precursor material on phase transition and stability of sintered $La_2Mo_2O_9$.

Keywords: Ceramics; Oxide materials; Ionic conduction; Phase transitions

1. Introduction

Oxygen-ion conductors have been extensively studied due to their use in oxygen sensors, oxygen pumps, oxygen-permeable membranes, and as solid electrolyte in high-temperature solid oxide fuel cells [1,2]. These materials may have different crystalline structures such as fluorite, pyrochlore, deficient perovskite, Aurivillius, brownmillerite, and apatite [2]. Recently a new family of oxygen-ion conductors based on a lanthanum molybdate mixed oxide was discovered [3]. The crystalline structure of $La_2Mo_2O_9$ from room temperature up to the phase transition temperature (∼580 °C), α-$La_2Mo_2O_9$, exhibits a slight monoclinic distortion and a large superstructure relative to the high-temperature cubic, β-$La_2Mo_2O_9$, phase [4]. The ionic conductivity of α-$La_2Mo_2O_9$ is about two orders of magnitude lower than that of β-$La_2Mo_2O_9$, which is slightly higher than that of the best yttria-stabilized zirconia solid electrolyte [3]. The mechanism of ionic conduction was explained on the basis of a lone pair substitution (LPS) concept [5]. Several works have shown that the phase transition may be partially or totally suppressed by suitable substitutions of La and/or Mo [3,6–12]. In particular, partial substitution of Mo for W has proved to be quite effective to avoid reduction of $La_2Mo_2O_9$ due to the change of molybdenum valence and, consequently, improves the stability of this compound in reducing environments [8].

In most of these works, solid state reactions between the starting oxides were employed to obtain the final compound. Only few studies have used solution techniques like sol–gel [13–15], polymeric precursors [16], freeze-drying of coprecipitated gels [17] and combustion of a polyacrylamide gel [18]. In general, solution methods give rise to very small particles, usually in the nanosize range with enhanced reactivity and chemical homogeneity. Moreover, reduction of the particle size towards the nanosize range may change drastically the microstructure-related properties of oxide materials. Experimental evidence of the particle size effect on dc conductivity of $La_2Mo_2O_9$ has been shown by comparing conductivity results obtained for submicron crystalline and microcrystalline specimens [14].

Considering the possible use of this ceramic compound as a solid electrolyte, several requirements must be fulfilled. In this context, any enhancement in the physical properties of $La_2Mo_2O_9$ by the use of improved methods of synthesis and

* Corresponding author. Tel.: +55 11 38169343; fax: +55 11 38169370.
E-mail address: enavarro@usp.br (E.N.S. Muccillo).

0925-8388/$ – see front matter © 2006 Elsevier B.V. All rights reserved.
doi:10.1016/j.jallcom.2006.10.001

processing is highly desirable. In this work, the effect of particle size on formation of the high-temperature β-$La_2Mo_2O_9$ phase and the stability of the sintered material were studied by X-ray diffraction, transmission electron microscopy, differential thermal analysis and impedance spectroscopy on materials prepared by solid state reactions from crystallized precursors.

2. Experimental details

La_2O_3 (99.9%, IPEN, Brazil) and MoO_3 (99%, Alfa Aesar) were the starting materials. The lanthanum oxide was synthesized at our Institute from a cerium-rich concentrate by the ion exchange resin and the fractioned precipitation techniques. A lanthanum nitrate solution was prepared by dissolving La_2O_3 in a hot nitric acid solution under stirring. The molybdenum nitrate solution was prepared in a similar way as that of lanthanum nitrate, except by the addition of a small amount of hydrogen peroxide. A mixed nitrate solution was then prepared by mixing under stirring the nitrate solutions in the stoichiometric proportion. This mixed nitrate was kept at ∼80 °C to reduce the volume of the precursor solution. The semi-dried material was then stored in an oven at 45 °C to promote the solvent evaporation along with crystallization of particles. The crystallized precursor was calcined at a temperature chosen from thermal analysis results, pressed into pellets and sintered at 950 °C for 24 h. For comparison purposes, the $La_2Mo_2O_9$ compound was also prepared by the mixing of starting oxides method. In this case, stoichiometric proportions of La_2O_3 and MoO_3 were mixed in an agate mortar, calcined twice at 550 °C for 6 h with intermediate grinding, pressed and sintered at 950 °C for 24 h.

The thermal decomposition of the crystallized precursor was followed by simultaneous thermogravimetry, TG, and differential thermal analysis, DTA (STA409, Netzsch) from room temperature up to 700 °C, heating at a rate of 5 °C min^{-1} in a dynamic atmosphere of synthetic air. In all experiments α-alumina was used as reference material. Powder materials were characterized by Fourier transform infrared spectroscopy, FT-IR (Magna IR 560, Nicolet), in the 400–4000 cm^{-1} spectral range. Specimens were mixed to KBr for this analysis. Transmission electron microscopy study was performed on a Jeol 200C microscope operating at 200 kV. Crystalline structures were identified by standard X-ray diffraction experiments using a diffractometer (D8 Advance, Bruker-AXS) equipped with Ni-filtered Cu Kα radiation source. Typical experimental conditions were 40 kV and 40 mA, and scans were conducted at a sampling interval of 0.05° and counting time of 10 s in the 15–75° 2θ range. Phase transition studies in sintered specimens were carried out by differential thermal analysis (Labsys, Setaran) with heating and cooling rates of 20 °C min^{-1}. Platinum paste (A308, Demetron) was painted onto large surfaces of specimens and baked at 800 °C for 1 h to act as electrode material for electrical measurements. Impedance spectroscopy measurements were carried out on sintered pellets in the 5 Hz to 13 MHz frequency range using a LF 4192A impedance analyzer (Hewlett Packard) connected via HPIB to a 362 HP model controller. The applied excitation signal was 100 mV. Isobaric impedance measurements were carried out in the 400–600 °C temperature range in a homemade alumina sample holder inserted in a tubular furnace (Lindberg Blue M). Impedance measurements were also carried out under controlled oxygen partial pressures from 1 to ∼10^{-6} atm at a fixed temperature of 700 °C using an YSZ electrochemical oxygen pump and sensor system connected to the impedance analyzer [19].

3. Results and discussion

3.1. Powder characterization

TG and DTA curves due to the decomposition reaction of the crystallized mixture of molybdenum and lanthanum nitrates are shown in Fig. 1. The weight loss occurs in several steps up to 460 °C, and beyond this temperature it is negligible. The total weight loss (44%) was lower than the theoretical value because the decomposition reaction started during crystallization at 45 °C. The DTA curve shows several thermal events. The

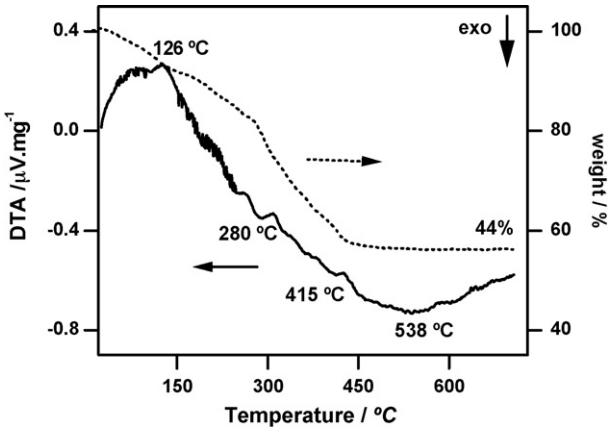

Fig. 1. TG and DTA curves of a crystallized mixture of Mo and La nitrates.

first endothermic peak (∼126 °C) is related to sample dehydration. The thermal decomposition of nitrates occurs at ∼280 °C. Another exothermic peak at ∼415 °C may be attributed to the elimination of decomposition products and formation of lanthanum oxycarbonate [20]. The broad exothermic event with maximum at ∼538 °C may be assigned to the formation of $La_2Mo_2O_9$, as will be shown below by FT-IR and X-ray diffraction measurements. From this result a calcination temperature of 550 °C was chosen.

FT-IR spectra of the crystallized precursor after several heat treatments are shown in Fig. 2. The main absorption bands after 460 °C for 1 min (Fig. 2a) are related to nitrate, oxynitrate and oxycarbonate groups. It is worth noting, however, absorption bands due to metal–oxygen (M–O) bonds at wavenumbers lower than 950 cm^{-1}. After calcination at 550 °C for 3 h (Fig. 2b), absorption bands related to intermediate compounds have disappeared. The main absorption bands are detected at ∼916, ∼820 and ∼719 cm^{-1}, which are assigned to $La_2Mo_2O_9$ [16]. This result suggests that the decomposition of lanthanum oxycarbonate is accelerated by the formation of $La_2Mo_2O_9$ compound. Calcinations of the precursor material for 6 h (Fig. 2c) and 12 h

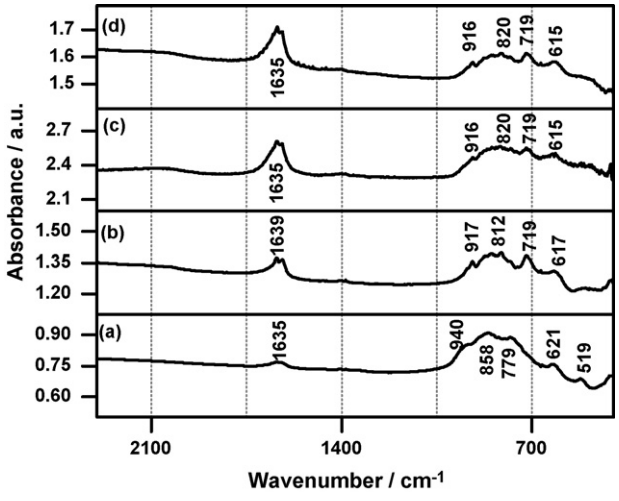

Fig. 2. FT-IR spectra of calcined materials: (a) 460 °C for 1 min, (b)–(d) 550 °C for 3, 6 and 12 h, respectively.

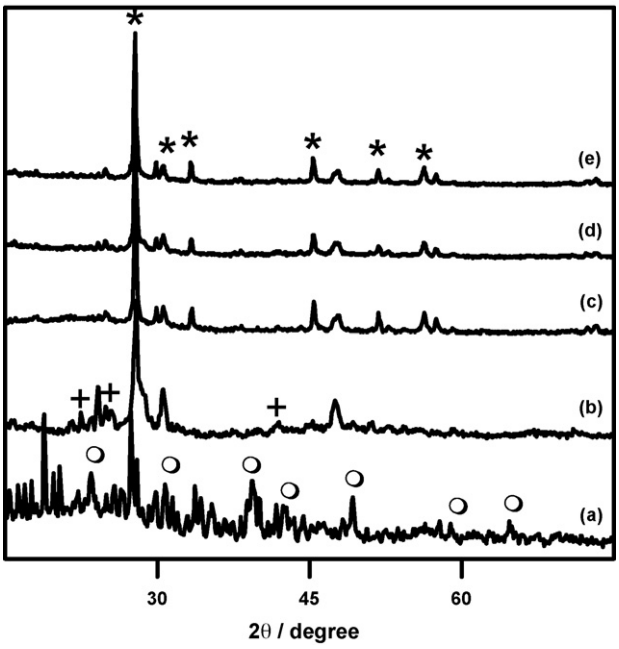

Fig. 3. XRD patterns of (a) crystallized La–Mo precursor, and after calcination at (b) 460 °C for 1 min, (c) 550 °C for 3 h, (d) 550 °C for 6 h and (e) 550 °C for 12 h. Lanthanum nitrate (◯), lanthanum oxycarbonate (+), and β-$La_2Mo_2O_9$ (*).

(Fig. 2d) did not produce any additional change in the type of chemical bond already formed.

Fig. 3 shows X-ray diffraction patterns of powder materials. The mixture of lanthanum and molybdenum nitrates (Fig. 3a) exhibits diffraction peaks of $La(NO_3)$ (ICDD 24-1112), $LaONO_3$ (ICDD 47-0890) and $La_2O_2CO_3$ (ICDD 37-0804). This result indicates the formation of lanthanum oxycarbonate at a lower temperature than expected from thermal analysis [20]. Then, some interaction between lanthanum and molybdenum must have occurred during crystallization. After calcination at 460 °C for 1 min, the two diffraction peaks with higher intensities of the cubic β-$La_2Mo_2O_9$ phase (ICDD 28-0509) may be observed (Fig. 3b) along with those of $La_2O_2CO_3$ and $La_2O(CO_3)_2$ (ICDD 32-0409). The X-ray diffraction pattern of the material calcined at 550 °C for 3 h (Fig. 3c) shows all reflections of $La_2Mo_2O_9$. Small intensity and non-identified peaks may also be seen in these patterns. Increase of the calcination time to 6 h (Fig. 3d) and 12 h (Fig. 3e) did not produce any change in the diffraction pattern in agreement with FT-IR spectra. This result indicates that no additional changes occur in the phase content with prolonged time of heat treatment at this temperature. Therefore, all subsequent calcinations were carried out for 3 h at 550 °C. Although α-$La_2Mo_2O_9$ is known to have a monoclinic symmetry, the distortion in the X-ray diffraction pattern is reported to be too small to be detected under standard X-ray measurements. Therefore, results shown in Fig. 3 indicate that the calcined powder possibly consists of a mixture of α- and β-$La_2Mo_2O_9$.

The room temperature bright field image of Fig. 4 shows that the calcined powder consists of agglomerated nanosized particles with polygonal shape. The electron diffraction pattern

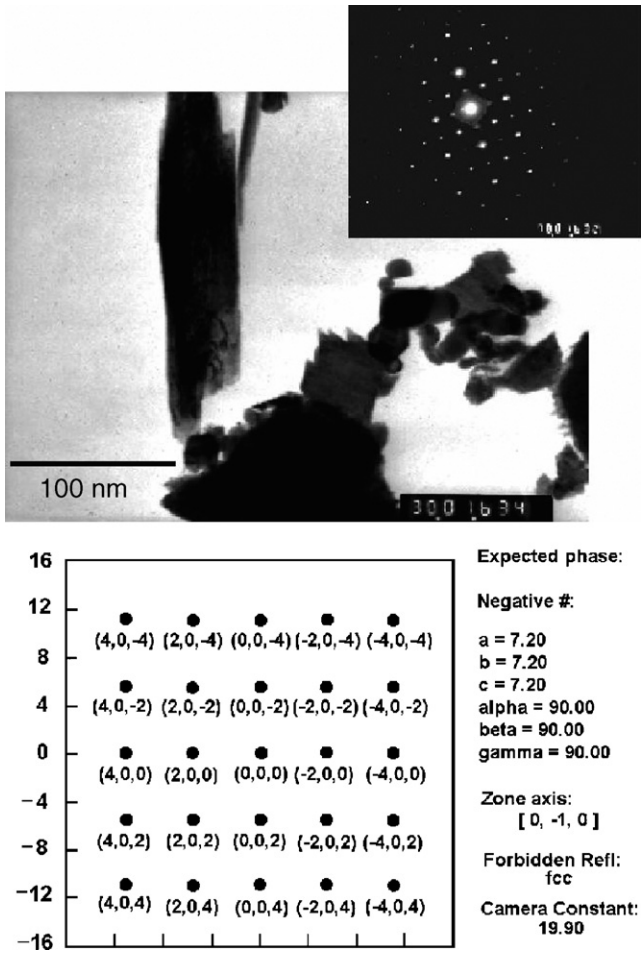

Fig. 4. Bright-field TEM image, electron diffraction pattern and results from fitting the diffraction pattern.

from some of these particles reveals only intense spots. One of them, shown in Fig. 4 and indexed using DIFPAT software (version 06.01) [21], indicates a cubic unit cell (space group $P2_13$) with lattice parameter equal to 7.20 Å. From a statistical viewpoint, this result evidences the cubic symmetry of some powder particles.

The stabilization of crystallographic phases in crystalline materials is known to be influenced by the size of particles. In general, the high-temperature phase is stabilized at lower temperatures with decreasing the particle size. For some materials, the predicted reduction of the temperature for phase stabilization can lead to a critical particle size, as observed in zirconia-based solid electrolytes. In this context, results shown in Figs. 3 and 4 may be understood as a consequence of the small size of the particles prepared from nitrate precursors. The metastable cubic phase at room temperature has been observed in quenched $La_2Mo_2O_9$ single crystals [22].

3.2. Sintered materials characterization

The characterized powder was pressed into pellets and sintered at 950 °C for 24 h. Fig. 5 shows a representative EDS spectrum of a fractured surface of $La_2Mo_2O_9$ pellet.

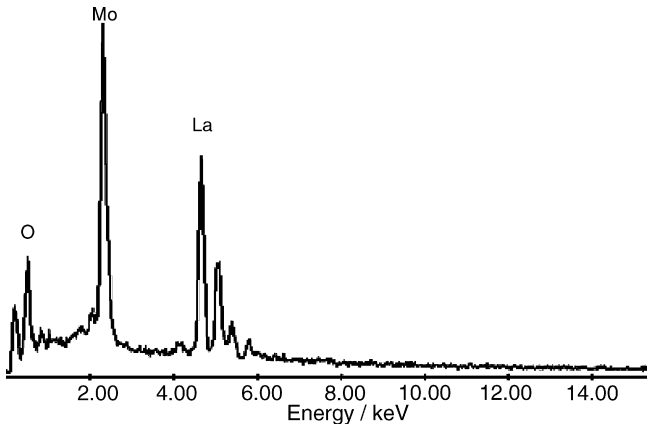

Fig. 5. EDS spectrum of a micro-region (fracture surface) of sintered $La_2Mo_2O_9$.

Several micro-regions were analyzed and an average elemental content was determined. In this spectrum, peaks corresponding to the energies of Kα emission of O and Lα emissions of La and Mo are indicated. The semi-quantitative determination for the ratio Mo/La (wt.%) resulted in an average value of 0.69 corroborating the stoichiometry of the synthesized compound. This result ensures that no important impurity is present in sintered $La_2Mo_2O_9$.

Impedance diagrams of a sintered specimen at three temperatures are shown in Fig. 6. In this figure, the imaginary part ($-Z''$) is plotted as a function of the real part (Z') of impedance. Numbers over experimental points are the logarithm of frequency (Hz). The impedance diagrams consist of one semicircle at high frequency and a spike for decreasing frequencies. The high-frequency semicircle is due to the electrical transport of charge carriers in the solid electrolyte, whereas the spike may be assigned to electrode polarization. The effect of sintering temperature on the shape of impedance diagrams in $La_2Mo_2O_9$ has been shown [17]. Thus, it is reasonable to assume that the grain boundaries semicircle overlaps with the semicircle due to electrode polarization in this case. In this figure, (a)–(c) indicate typical impedance diagrams measured before, at and after the $\alpha \rightleftharpoons \beta$ phase transition in $La_2Mo_2O_9$ sintered compound.

The Arrhenius plot of the electrical conductivity in the 400–600 °C temperature range is shown in Fig. 7. Different symbols in this figure refer to experimental values measured in different heating cycles. This procedure was undertaken to ensure that the specimen being measured was thermally stable in the whole temperature range. The electrical conductivity increases with increasing temperature as usual in a thermally activate process. At a given temperature, there is a change of slope of the conductivity data with an increase of that value by, approximately, one order of magnitude, due to the structural phase transition. The reversible phase transition occurs at a lower temperature range (530–555 °C during heating) than that of specimens prepared by mixing of starting oxides [3]. Moreover, the phase transition is not as sharp as observed for $La_2Mo_2O_9$ prepared by the conventional mixing of oxides [3]. Therefore, it can be concluded that the relatively small particle

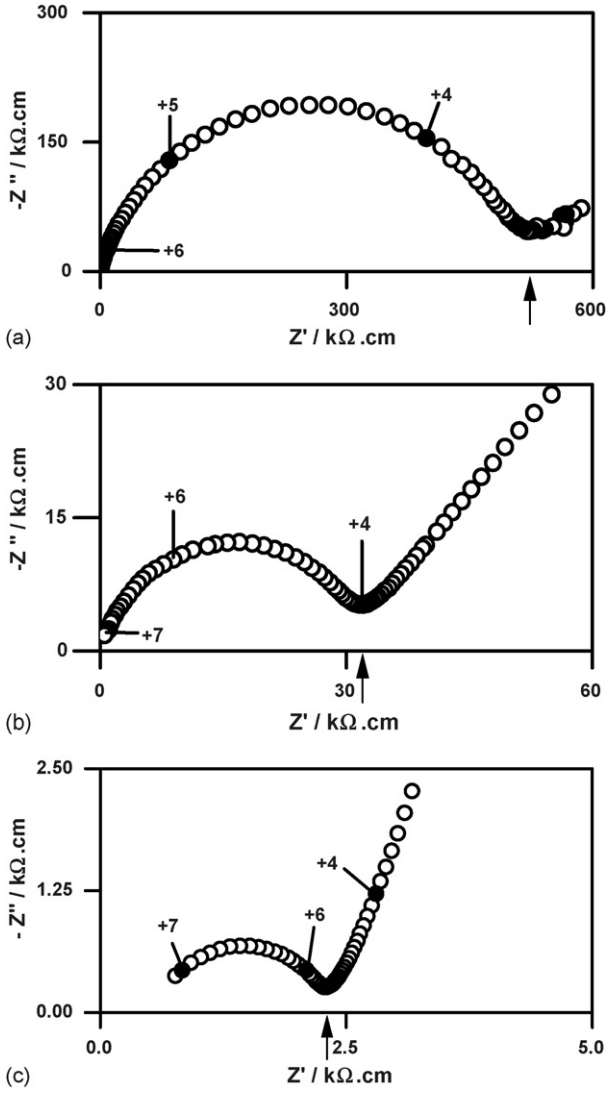

Fig. 6. Impedance spectroscopy diagrams of sintered $La_2Mo_2O_9$. Measuring temperatures: (a) 439 °C, (b) 505 °C, and (c) 554 °C.

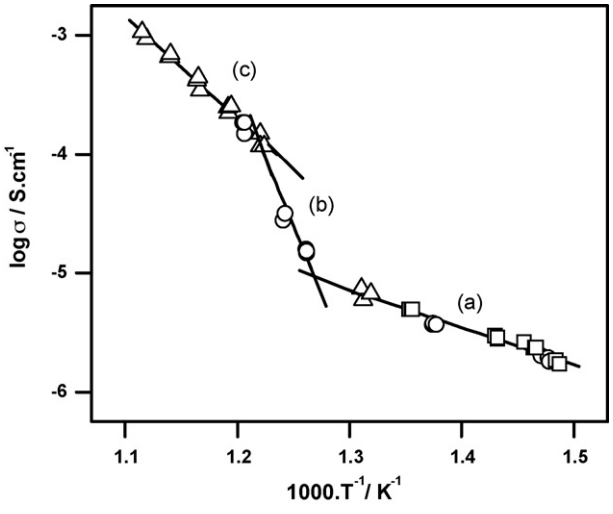

Fig. 7. Arrhenius plot of the electrical conductivity of sintered $La_2Mo_2O_9$ compound.

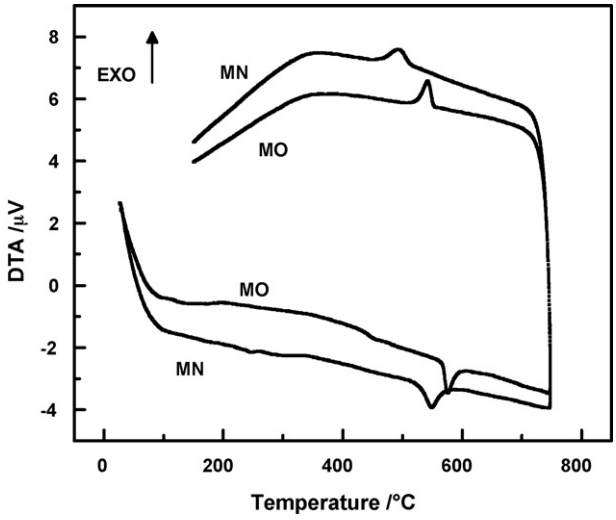

Fig. 8. Differential thermal analysis of sintered $La_2Mo_2O_9$ compound prepared by the mixture of oxides (MO) and nitrates (MN).

size of the crystallized precursor is responsible for differences in the magnitude of the electrical conductivity and the phase transition behavior of the sintered material. Results obtained for specimens prepared by mixing of oxides, not shown here, are similar to those already published [3,17,18].

The phase transition was also studied by differential thermal analysis. In this case, the sintered pellet was sliced into several small pieces, and this material was heated at a rate of 20 °C min^{-1} from room temperature up to 750 °C. Fig. 8 shows DTA curves corresponding to a heating–cooling cycle for specimens prepared from the mixture of starting oxides (MO) and nitrates (MN). A characteristic endothemic peak during heating and an exothermic peak during cooling of the samples were detected due to the $\alpha \rightleftharpoons \beta$ phase transition.

The thermal hysteresis characterizes this phase transition as a first order one. However, the hysteresis seems to be larger in DTA than in conductivity measurements probably due to different heating and cooling rates. During heating, the peak temperatures of phase transition were 575 and 548 °C for specimens prepared from mixtures of oxides (MO) and nitrates (MN), respectively. This considerable reduction of the phase transition temperature of $La_2Mo_2O_9$ in MN specimens, assigned to a particle size effect, agrees with results of electrical conductivity (Fig. 7).

Resistance values measured at a fixed frequency of 10 kHz were converted to conductivity, σ. Fig. 9 shows conductivity results at different oxygen partial pressures for specimens prepared by solid state sintering using different precursor materials. At a fixed temperature of 700 °C the electrical conductivity of the specimen prepared from starting oxides (Fig. 9a) increases with decreasing oxygen partial pressure. Similar results were observed in previous works [18,23], where the n-type conduction behavior was associated with the redox properties of Mo^{6+} under reducing atmospheres. Changes of oxygen stoichiometry and of the Mo valence are prone to occur in pure $La_2Mo_2O_9$ limiting the applicability of this ionic conductor. It has already been shown that oxygen deficiency can produce different phases

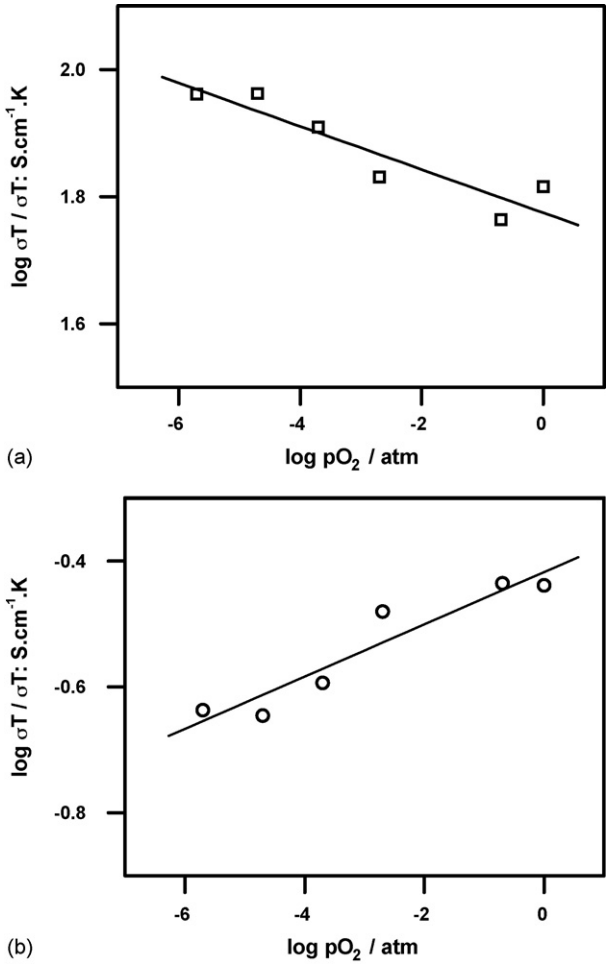

Fig. 9. Variation of the electrical conductivity with oxygen partial pressure of sintered $La_2Mo_2O_9$ prepared from starting oxides (a) and nitrates (b).

in this material such as $La_{2.4}Mo_{1.6}O_8$ with average valence of Mo equal to 5.5 [24], and $La_7Mo_7O_{30}$ [24,25].

The isothermal conductivity for specimens prepared from mixed nitrate (Fig. 9b) shows a quite different behavior. The electrical conductivity increases with increasing oxygen partial pressure indicating a more complex relationship among the oxygen content, the Mo valence and the crystallographic phase in the sintered material. The explanation of this behavior is outside the scope of this paper, but it demonstrates the need of further experiments to clarify the mechanism of defect formation taken into account both thermodynamic and kinetic effects in this material.

4. Conclusions

The $La_2Mo_2O_9$ compound was prepared by crystallization of a precursor nitrate solution at relatively low-temperatures and short times compared to the conventional method of mixing of starting oxides. The material calcined at 550 °C consists of the low-temperature monoclinic phase and the metastable cubic β-$La_2Mo_2O_9$. Sintered pellets have a lower phase transition temperature due to the smaller size of the starting particles.

Acknowledgements

To FAPESP, CNPq and CNEN for financial supports. To Drs. A.H.A. Bressiani and F.C. Fonseca for TEM and DTA analyses, respectively. R.A. Rocha acknowledges FAPESP (01/12269-7) for the scholarship.

References

[1] B.C.H. Steele, Mater. Sci. Eng. B 13 (1992) 79–87.
[2] J.B. Goodenough, Ann. Rev. Mater. Res. 33 (2003) 91–128.
[3] P. Lacorre, F. Goutenoire, O. Bohnke, R. Retoux, Y. Laligant, Nature 404 (2000) 856–858.
[4] F. Goutenoire, O. Isnard, R. Retoux, P. Lacorre, Chem. Mater. 12 (2000) 2575–2580.
[5] P. Lacorre, Solid State Sci. 2 (2000) 755–758.
[6] X.P. Wang, Q.F. Fang, Solid State Ionics 146 (2002) 185–193.
[7] Q.F. Fang, X.P. Wang, Z.S. Li, G.G. Zhang, Z.G. Yi, Mater. Sci. Eng. A 370 (2004) 365–369.
[8] S. Georges, F. Goutenoire, Y. Laligant, P. Lacorre, J. Mater. Chem. 13 (2003) 2317–2321.
[9] S. Basu, P.S. Devi, H.S. Maiti, Appl. Phys. Lett. 85 (2004) 3486–3488.
[10] S. Georges, F. Goutenoire, O. Bohnke, M.C. Steil, S.J. Skinner, H.-D. Wiemhöfer, P. Lacorre, J. N. Mater. Electrochem. Syst. 7 (2004) 51–57.
[11] J. Yang, Z. Gou, Z. Wen, D. Yan, Solid State Ionics 176 (2005) 523–530.
[12] X.P. Wang, Z.J. Cheng, Q.F. Fang, Solid State Ionics 176 (2005) 761–765.
[13] W. Kuang, Y. Fan, K. Yao, Y. Chen, J. Solid State Chem. 140 (1998) 354–360.
[14] Z.G. Yi, Q.F. Fang, X.P. Wang, G.G. Zhang, Solid State Ionics 160 (2003) 117–124.
[15] U. Kersen, R. Keiski, J. Nanosci. Nanotechnol. 5 (2005) 1734–1736.
[16] R.A. Rocha, E.N.S. Muccillo, Chem. Mater. 15 (2003) 4268–4272.
[17] D. Marrero-López, J. Canales-Vázquez, J.C. Ruiz-Morales, A. Rodriguez, J.T.S. Irvine, P. Núñez, Solid State Ionics 176 (2005) 1807–1816.
[18] A. Tarancón, T. Norby, G. Dezanneau, A. Morata, F. Peiró, Electrochem. Solid State Lett. 7 (2004) A373–A375.
[19] M.C. Steil, F.C. Fonseca, Y.V. França, J.F.Q. Rey, E.N.S. Muccillo, R. Muccillo, Ceramica 48 (2002) 146–152.
[20] B. Klingenber, M.A. Vannice, Chem. Mater. 8 (1996) 2755–2768.
[21] G. Carpenter, L. Benkis, CANMET, Ottawa, Canada, 1990.
[22] V.I. Voronkova, V.K. Yanovskii, E.P. Kharitonova, Crystallogr. Rep. 50 (2005) 874–876.
[23] D. Marrero-López, J. Canales-Vásquez, J.C. Ruiz-Morales, J.T.S. Irvine, P. Núñez, Electrochim. Acta 50 (2005) 4385–4395.
[24] D. Marrero-López, J.C. Ruiz-Morales, D. Pérez-Coll, P. Núñez, J.C.C. Abrantes, J.R. Frade, J. Solid State Electrochem. 8 (2004) 638–643.
[25] F. Goutenoire, R. Retoux, E. Suard, P. Lacorre, J. Solid State Chem. 142 (1999) 228–235.